

UAV as Urban Construction Change Monitor: A New Benchmark and Change Captioning Model

Yupeng Gao¹, Tianyu Li¹, Guoqing Wang¹, and Yang Yang¹

University of Electronic Science and Technology of China, Chengdu, China
202411081510@std.uestc.edu.cn, cosmos.yu@hotmail.com,
gqwang0420@uestc.edu.cn, yang.yang@uestc.edu.cn

Abstract. Remote Sensing Image Change Captioning (RSICC) aims to generate spatially grounded natural language descriptions of scene evolution from bi-temporal imagery, moving beyond binary change masks toward semantic-level understanding. However, existing methods rely on implicit feature differencing without explicitly modeling structured change semantics, and struggle to reconcile the conflicting representation demands of change detection and caption generation. In addition, current benchmarks provide limited coverage of high-resolution urban construction scenarios. To address these challenges, we propose PTNet, a prototype-guided task-adaptive framework for joint change captioning and detection. PTNet explicitly models structured change semantics through a learnable prototype bank that guides cross-temporal interaction, disentangles task-specific representations via multi-head gating, and injects detection-derived spatial priors into caption generation, enabling coherent semantic correspondence while preserving fine-grained spatial sensitivity. Furthermore, we construct UCCD, a large-scale UAV-based benchmark comprising 9,000 high-resolution image pairs and 45,000 annotated sentences for urban construction monitoring. Extensive experiments on UCCD and WHU-CDC demonstrate that PTNet consistently outperforms existing methods. The dataset and source code are publicly available at <https://github.com/G124556/ptnet>.

Keywords: Change captioning · Prototype learning · Task-adaptive decoupling · UAV remote sensing

1 Introduction

The continuous advancement of remote sensing technologies has driven rapid progress in multi-temporal analysis tasks such as change detection and change captioning [1–3]. Unlike traditional change detection that only localizes changed regions, Remote Sensing Image Change Captioning (RSICC) advances toward semantic-level understanding by generating natural language descriptions of scene evolution, providing interpretable information for land-use auditing, urban monitoring, and emergency response [4], and enabling seamless integration into higher-level reasoning pipelines [5].

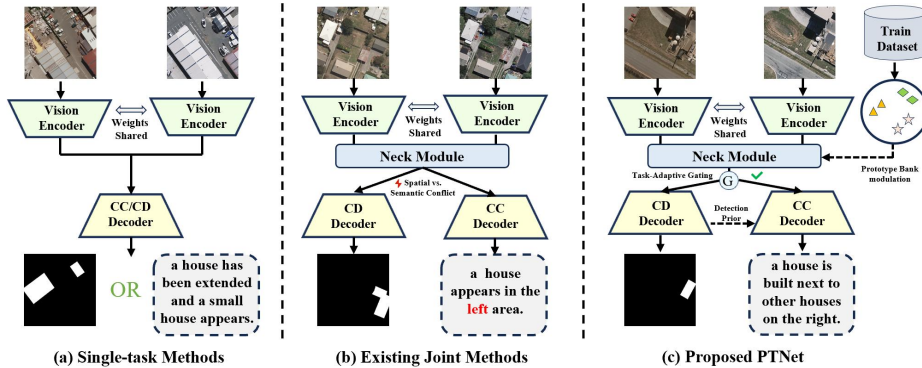


Fig. 1: (a) single-task methods that produce either a change mask or a caption, (b) existing joint methods that suffer from feature conflicts and inaccurate descriptions, and (c) the proposed PTNet, which introduces prototype-guided semantic modeling and task-adaptive feature decoupling for accurate and spatially faithful change captioning.

Existing RSICC methods follow an encoder–decoder paradigm to model cross-temporal visual differences. While subsequent advances incorporating Transformers [6, 7], state space models [8], diffusion models [9], and large language models [10, 11] have progressively enhanced semantic alignment, and joint detection–captioning frameworks [12–14] leverage spatial cues to improve caption quality, two fundamental limitations persist. First, most approaches rely on implicit feature differencing without explicitly modeling structured change-type semantics, limiting accurate temporal correspondences in complex scenes [15]. Second, change detection and captioning impose inherently incompatible representation demands—spatial precision versus semantic abstraction—and simple shared-feature or parallel-branch designs fail to resolve this granularity mismatch [16], as illustrated in Fig. 1.

Beyond methodology, existing benchmarks provide insufficient coverage of urban construction scenarios, constrained in annotation scale and scene diversity [17]. Most focus on natural disaster or agricultural changes, with sparse samples capturing fine-grained urban dynamics such as illegal building expansion and incremental land-use transitions, restricting systematic study in realistic urban environments.

To address these challenges, we propose **PTNet** (Prototype-Guided Task-Adaptive Network), a unified framework for joint change detection and captioning, where captioning serves as the primary objective and detection provides spatial grounding. PTNet models structured change semantics via learnable change-type prototypes for cross-temporal alignment, and employs task-adaptive gating to produce sub-task-aware representations. A lightweight mask encoder injects detection-derived spatial priors into caption generation, while a CLIP-based contrastive objective [18, 19] enforces cross-modal consistency. In addition, we con-

struct UCCD, a large-scale UAV-based urban change captioning benchmark. The main contributions are as follows:

1. We introduce **PG-CAI** as a core semantic modeling component of PTNet, which clusters training-set change features into learnable change-type prototypes to guide cross-temporal attention and enable explicit semantic-level temporal correspondences and structured semantic priors for both sub-tasks.
2. We develop **TAMG** module to learn task-adaptive feature representations at the attention-head granularity, enabling detection and captioning to maintain appropriate spatial and semantic sensitivities within a unified framework, alleviating the conflict from their incompatible feature requirements.
3. A lightweight mask encoder is incorporated into PTNet to inject detection-derived spatial priors into caption generation, while a CLIP-based contrastive objective enforces cross-modal semantic consistency.
4. We construct **UCCD**, a large-scale benchmark comprising 9,000 high-resolution low-altitude UAV image pairs and 45,000 annotated sentences for fine-grained urban construction change understanding, providing both detection annotations and detailed semantic descriptions. To our knowledge, UCCD is the first low-altitude UAV-based benchmark specifically designed for joint change detection and captioning in urban construction environments.

2 Related Work

Remote sensing change detection has evolved from CNN-based approaches [20–23] to Transformer-based architectures [24, 25], with methods like BIT [26] and ChangeFormer [27] improving localization accuracy via self-attention. However, their outputs remain limited to binary change masks. To address this, RSICC has emerged as a cross-modal task generating natural language descriptions of semantic changes [28].

Early RSICC methods established the encoder–decoder paradigm for cross-temporal visual understanding. RSICCformer [29] introduced dual-branch Transformers to model bi-temporal feature interactions, while Chg2Cap [30] incorporated attentive difference modules to highlight changed regions. Subsequently, PromptCC [31] introduced a prompt-based decoupling paradigm to disentangle change-relevant semantics; RSCaMa [32] leveraged state space models to capture long-range temporal dependencies; and MADiffCC [33] employed diffusion models to enrich caption diversity. More recently, Semantic-CC [34] and KCFI [35] incorporated large language models to produce richer semantic descriptions. Despite these advances, all of the above methods rely on implicit feature differencing without explicitly modeling structured change-type semantics, and cannot leverage the complementary spatial supervision from change detection.

With the advancement of MLLMs [36–41], ChangeChat [42], CDChat [43], and BTCChat [44] have progressively enriched semantic depth and temporal modeling in change understanding, demonstrating that integrating LLM reasoning with change-aware perception is a promising direction—motivating our LLM-based captioning branch with contrastive cross-modal alignment.

Beyond pure captioning, another active direction jointly models detection and captioning to leverage region-level supervision for more spatially faithful language generation [12]. Most existing approaches adopt a shared backbone with dual task-specific heads, yet several design limitations remain. Shi *et al.* [13] employs largely shared representations without explicitly accounting for task-specific feature sensitivities; Wang *et al.* [45] introduces detection cues but does not effectively propagate spatial priors into the captioning branch; and Liu *et al.* and Li *et al.* [14, 15] do not explicitly model structured change types nor provide fine-grained task-aware representation control. In contrast, PTNet explicitly decouples task-specific representations via TAMG and injects detection spatial priors through mask-guided encoding, enabling the two tasks to mutually reinforce each other.

3 Methodology

3.1 Overall Framework

The overall architecture of PTNet, illustrated in Fig. 2. Given a bi-temporal remote sensing image pair $(\mathcal{I}_1, \mathcal{I}_2) \in \mathbb{R}^{H \times W \times 3}$, our primary objective is to generate accurate and spatially-aware natural language descriptions $\mathbf{T} = [w_1, \dots, w_L]$, while auxiliarily producing a change detection mask $\mathbf{M} \in \{0, 1\}^{H \times W}$ as a spatial localization.

We employ a pre-trained CLIP Vision Encoder (ViT-L/14) as the shared backbone, fine-tuned via LoRA [46], to extract hierarchical feature representations from the 6th, 12th, 18th, and 24th transformer layers for each input image:

$$\mathbf{F}_j^i = \Phi_v^i(\mathcal{I}_j), \quad j \in \{1, 2\}, i \in \{1, 2, 3, 4\}, \quad (1)$$

where j denotes the temporal phase, i denotes the hierarchy level, and $\mathbf{F}_j^i \in \mathbb{R}^{N \times D}$. The Prototype-Guided Change-Aware Interaction (PG-CAI) module maintains learnable change-type prototypes $\mathbf{P} \in \mathbb{R}^{K \times N \times D}$ to guide prototype-modulated bidirectional cross-temporal attention, producing change-aware bi-temporal features $\{\mathbf{G}_1^i, \mathbf{G}_2^i\}$. The Task-Adaptive Multi-head Gating (TAMG) module then learns differentiated gating weights at the attention-head granularity to separately generate detection-oriented features \mathbf{O}^d and captioning-oriented features \mathbf{O}^c via cross-level adaptive fusion. In the task-specific decoding stage, an FPN [47] detection branch decodes \mathbf{O}^d into a change probability map $\hat{\mathbf{M}}$, while a captioning branch built on Qwen2-1.5B-Instruct, fine-tuned via LoRA, encodes fine-grained spatial features extracted from the FPN detection branch into compact detection tokens, which are concatenated with \mathbf{O}^c to inject spatial localization priors into caption generation. Finally, a vision-language semantic alignment loss based on InfoNCE pulls the captioning visual representations toward their corresponding CLIP text embeddings, ensuring consistency with the language semantic space.

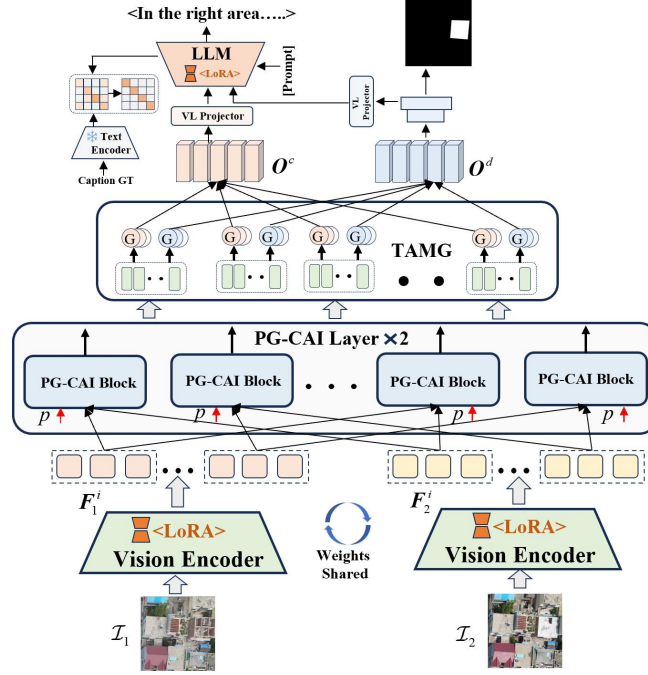


Fig. 2: Overall architecture of the proposed PTNet.

3.2 Prototype-Guided Change-Aware Interaction

Prototype Initialization As depicted in Fig. 3(a), we initialize $\mathbf{P} \in \mathbb{R}^{K \times N \times D}$ offline using the training set, where K is the number of prototype clusters, N is the number of spatial tokens, and D is the feature dimension. For each training sample s , we compute difference features using the second-level hierarchical features \mathbf{F}_j^2 extracted from the 12th transformer layer of the CLIP Vision Encoder, which captures mid-level semantic structure while retaining sufficient spatial resolution for change localization. A compact representation $\mathbf{z}^{(s)} \in \mathbb{R}^D$ is then obtained by mask-guided average pooling over changed pixels, or global average pooling for unchanged samples:

$$\mathbf{Z}^{(s)} = |\mathbf{F}_1^{2,(s)} - \mathbf{F}_2^{2,(s)}| \in \mathbb{R}^{N \times D}, \quad \mathbf{z}^{(s)} = \begin{cases} \text{AvgPool}(\{\mathbf{Z}_b^{(s)}\}_{b \in \Omega^{(s)}}) & \text{if } |\Omega^{(s)}| > 0 \\ \frac{1}{N} \sum_{b=1}^N \mathbf{Z}_b^{(s)} & \text{otherwise} \end{cases} \quad (2)$$

where $\Omega^{(s)} = \{b \mid \mathbf{M}_b^{(s)} = 1\}$ denotes the set of changed pixel indices. K-means clustering on $\{\mathbf{z}^{(s)}\}_{s=1}^S$ yields K cluster centers $\{\mathbf{c}_k^0\}_{k=1}^K$, naturally covering one “no-change” pattern and $K-1$ distinct change types.

Since the pooling operation discards spatial structure, we recover it by re-expanding each aggregated vector into a dense spatial map $\tilde{\mathbf{Z}}^{(s)} \in \mathbb{R}^{N \times D}$ via

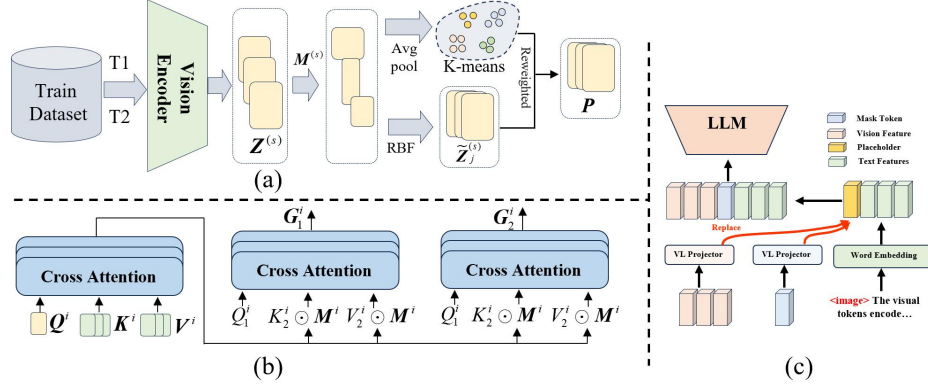


Fig. 3: (a) **Prototype bank construction:** training-set difference features are clustered via K-means and spatially recovered via RBF interpolation to form the learnable prototype bank $\mathbf{P} \in \mathbb{R}^{K \times N \times D}$. (b) **PG-CAI Block:** \mathbf{P} modulates bidirectional cross-attention between $\{\mathbf{F}_1^i, \mathbf{F}_2^i\}$, producing change-aware features $\{\mathbf{G}_1^i, \mathbf{G}_2^i\}$. (c) **Change Captioning Decoder:** change-aware features are projected into the LLM token space and concatenated with detection tokens for caption generation.

Radial Basis Function (RBF) interpolation [48]:

$$\tilde{\mathbf{Z}}_v^{(s)} = \sum_{l \in \Omega^{(s)}} w_{vl} \mathbf{Z}_l^{(s)}, \quad w_{vl} \propto \exp\left(-\frac{\|\mathbf{p}_v - \mathbf{p}_l\|^2}{2\sigma^2}\right), \quad (3)$$

where $\mathbf{p}_v, \mathbf{p}_l \in \mathbb{R}^2$ denote the 2D spatial coordinates of positions v and l respectively, and σ is the Gaussian bandwidth controlling interpolation smoothness. For unchanged samples where $\Omega^{(s)} = \emptyset$, the interpolation reduces to uniform spatial replication. Finally, prototypes are initialized by aggregating spatially recovered features weighted by soft cluster assignments:

$$\alpha_k^{(s)} = \frac{\exp(-\|\mathbf{z}^{(s)} - \mathbf{c}_k^0\|^2/\tau)}{\sum_{k'=1}^K \exp(-\|\mathbf{z}^{(s)} - \mathbf{c}_{k'}^0\|^2/\tau)}, \quad \mathbf{P}_k^0 = \sum_{s=1}^S \alpha_k^{(s)} \tilde{\mathbf{Z}}^{(s)}, \quad (4)$$

where τ is the temperature controlling assignment sharpness. The resulting prototype bank $\mathbf{P} = [\mathbf{P}_1; \dots; \mathbf{P}_K] \in \mathbb{R}^{K \times N \times D}$ is treated as a learnable parameter and jointly optimized with downstream tasks.

Prototype-Modulated Cross-Temporal Interaction As illustrated in Fig. 3(b), for each level i , we first construct change queries by fusing bi-temporal features and their difference:

$$\mathbf{U}^i = \text{MLP}([\mathbf{F}_1^i; \mathbf{F}_2^i; |\mathbf{F}_1^i - \mathbf{F}_2^i|]) \in \mathbb{R}^{N \times D}. \quad (5)$$

The query, key, and value projections are computed as:

$$\mathbf{Q}^i = \mathbf{U}^i \mathbf{W}_Q^i, \quad \mathbf{K}^i = \mathcal{R}(\mathbf{P} \mathbf{W}_K^i), \quad \mathbf{V}^i = \mathcal{R}(\mathbf{P} \mathbf{W}_V^i), \quad (6)$$

where $\mathcal{R}(\cdot)$ denotes the reshape operation that flattens the prototype bank $\mathbf{P} \in \mathbb{R}^{K \times N \times D}$ into $\mathbb{R}^{KN \times D}$ for attention computation. The modulation feature \mathbf{M}^i is then retrieved via:

$$\mathbf{M}^i = \text{Softmax}\left(\frac{\mathbf{Q}^i(\mathbf{K}^i)^T}{\sqrt{d_k}}\right) \mathbf{V}^i \in \mathbb{R}^{N \times D}, \quad (7)$$

\mathbf{M}^i encodes semantic priors about which change type each location belongs to, guiding bidirectional cross-temporal attention via element-wise modulation. The T1→T2 and T2→T1 directions are computed symmetrically:

$$\mathbf{Q}_a^i = \mathbf{F}_a^i \mathbf{W}_{Q,a}^i, \quad \mathbf{K}_b^i = (\mathbf{F}_b^i \odot \mathbf{M}^i) \mathbf{W}_{K,b}^i, \quad \mathbf{V}_b^i = (\mathbf{F}_b^i \odot \mathbf{M}^i) \mathbf{W}_{V,b}^i, \quad (8)$$

where $\{a, b\} \in \{\{1, 2\}, \{2, 1\}\}$ denotes the two directions of bidirectional attention. The output features are then obtained as:

$$\mathbf{G}_1^i = \text{Softmax}\left(\frac{\mathbf{Q}_1^i(\mathbf{K}_2^i)^T}{\sqrt{d_k}}\right) \mathbf{V}_2^i + \mathbf{F}_1^i, \quad \mathbf{G}_2^i = \text{Softmax}\left(\frac{\mathbf{Q}_2^i(\mathbf{K}_1^i)^T}{\sqrt{d_k}}\right) \mathbf{V}_1^i + \mathbf{F}_2^i, \quad (9)$$

where \odot denotes element-wise multiplication and the residual term preserves original features. This bidirectional block is stacked in two cascaded layers with independent parameters, yielding the final change-aware features $\{\mathbf{G}_1^i, \mathbf{G}_2^i\}_{i=1}^4$.

3.3 Task-Adaptive Multi-head Gating

Each change-aware feature \mathbf{G}_j^i is decomposed into H heads, and for each task $t \in \{d, c\}$, a head-wise sigmoid gate is applied:

$$g_{j,h}^{i,t} = \sigma(\mathbf{w}_{j,h}^{i,t} \cdot \mathcal{P}(\mathbf{G}_{j,h}^i) + b_{j,h}^{i,t}), \quad \tilde{\mathbf{G}}_{j,h}^{i,t} = g_{j,h}^{i,t} \cdot \mathbf{G}_{j,h}^i, \quad (10)$$

where $\mathcal{P}(\cdot)$ denotes global average pooling. All levels and temporal phases are then fused via learnable weights:

$$\mathbf{O}^t = \sum_{i=1}^4 \sum_{j=1}^2 \beta_j^{i,t} [\tilde{\mathbf{G}}_{j,1}^{i,t}; \dots; \tilde{\mathbf{G}}_{j,H}^{i,t}], \quad \beta_j^{i,t} = \frac{\exp(s_j^{i,t})}{\sum_{i',j'} \exp(s_{j'}^{i',t})} \quad (11)$$

yielding task-specific representations $\mathbf{O}^d, \mathbf{O}^c \in \mathbb{R}^{N \times D}$.

3.4 Task-Specific Decoders

Change Detection Decoder An FPN-based branch decodes \mathbf{O}^d into a change probability map $\hat{\mathbf{M}} \in \mathbb{R}^{H \times W}$, supervised by binary cross-entropy:

$$\mathcal{L}_d = -\frac{1}{HW} \sum_{i,j} [\mathbf{M}_{ij} \log \hat{\mathbf{M}}_{ij} + (1 - \mathbf{M}_{ij}) \log(1 - \hat{\mathbf{M}}_{ij})]. \quad (12)$$

Change Captioning Decoder As illustrated in Fig. 3(c), to inject spatial localization priors into caption generation, we encode \mathbf{F}_{s2} , the high-resolution feature map from the finest level of the FPN detection branch, which retains fine-grained spatial details of changed regions, into compact detection tokens via adaptive pooling and a two-layer MLP:

$$\mathbf{D}_d = \text{MLP}(\text{Reshape}(\mathcal{A}(\mathbf{F}_{s2}, (H_m, W_m)))) \in \mathbb{R}^{B \times N_m \times K_d}, \quad N_m = H_m W_m. \quad (13)$$

Captioning features \mathbf{O}^c are projected to the LM input space and concatenated with detection tokens:

$$\mathbf{V}_{\text{comb}} = [\mathbf{D}_d; \mathbf{W}_c \mathbf{O}^c] \in \mathbb{R}^{B \times (N_m + N) \times D_{\text{LM}}}. \quad (14)$$

This concatenation strategy allows the language model to simultaneously attend to semantic change features from \mathbf{O}^c and explicit spatial grounding from \mathbf{D}_d , where the latter encodes the shape, extent, and spatial distribution of changed regions that visual features alone cannot precisely convey. \mathbf{V}_{comb} is fed into Qwen2-1.5B-Instruct, fine-tuned via LoRA to preserve pretrained linguistic knowledge while adapting to remote sensing change semantics. A task prompt instructing the model to describe observed changes based on change-aware and detection-derived tokens is used for autoregressive caption generation (see supp.).

3.5 Vision-Language Semantic Alignment

To align captioning visual representations with the CLIP semantic space, we apply InfoNCE contrastive loss, analogous to CLIP’s image-text contrastive learning but using the frozen CLIP text encoder as a fixed semantic anchor. Text embeddings are obtained via $\mathbf{e}_t = \Phi_t(\mathbf{T})$, and visual embeddings are derived by pooling the LM’s last-layer hidden states—which encode visually-grounded representations closer to natural language semantics than raw visual features—and projecting to the same space:

$$\mathbf{e}_v^c = \text{Linear} \left(\frac{1}{L} \sum_{l=1}^L \mathbf{h}_l^{\text{LM}} \right) \in \mathbb{R}^{d_t}, \quad \mathcal{L}_a = -\frac{1}{B} \sum_{b=1}^B \log \frac{\exp(\text{sim}(\mathbf{e}_v^{c,(b)}, \mathbf{e}_t^{(b)})/\tau)}{\sum_{b'=1}^B \exp(\text{sim}(\mathbf{e}_v^{c,(b)}, \mathbf{e}_t^{(b')})/\tau)}. \quad (15)$$

3.6 Training Objective and Strategy

The overall training objective jointly optimizes three losses, where the captioning branch minimizes token-level cross-entropy against ground-truth captions:

$$\mathcal{L}_{\text{tot}} = \lambda_1(t) \mathcal{L}_c + \lambda_2(t) \mathcal{L}_d + 0.3 \mathcal{L}_a, \quad \mathcal{L}_c = -\frac{1}{n} \sum_{i=1}^n \sum_{v=1}^V y_{i,v} \log y'_{i,v}. \quad (16)$$

Dynamic Weight Balancing. Following [49], $\lambda_1(t)$ and $\lambda_2(t)$ are adapted based on each task’s loss improvement rate:

$$\lambda_k(t) = \frac{2 \exp(w_k(t-1)/T)}{\sum_{i=1}^2 \exp(w_i(t-1)/T)}, \quad w_k(t-1) = \frac{\mathcal{L}_k(t-1)}{\mathcal{L}_k(t-2)}, \quad k \in \{1, 2\}, \quad (17)$$

where $T=2.0$ controls the sharpness of weight allocation, assigning higher weights to tasks with slower improvement.

4 UCCD Dataset

4.1 Data Collection and Preprocessing

This paper constructs a change detection and captioning dataset UCCD (Urban Change Captioning and Detection) oriented toward urban construction scenarios. Image data were collected in Xuzhou City, Jiangsu Province, China, using DJI drones with nadir viewing angles. The original resolution is 3024×4032 pixels with a spatial resolution of 6 cm/pixel. The temporal interval between each image pair is approximately 7 days, a time window that effectively captures urban construction dynamics. To ensure image registration accuracy, the Light-Glue [50] algorithm is employed for pixel-level alignment of all image pairs. After registration, the original images are cropped into 1024×1024 pixel sub-images using a sliding window strategy, and samples in which the changed region occupies less than 0.8% of the total image area are discarded to ensure sufficient change content. After the above processing, 9,000 high-quality image pairs are ultimately obtained, which are split into training, validation, and test sets at a ratio of 7:1:2.

4.2 Dataset Annotation

The dataset contains 6,645 changed image pairs and 2,355 unchanged image pairs, with category distribution reflecting actual patterns in short-term urban monitoring. Change types cover multiple dimensions including building construction/demolition/ renovation, temporary structure installation, solar facility installation, ground hardening and land use changes, and vegetation removal and planting. Table 1 compares UCCD with existing datasets. Figure 4 presents the full annotation pipeline and statistical analysis of the dataset.

Change Mask Annotation. All change masks are manually annotated by professional annotators to ensure precise spatial localization.

Text Caption Annotation. We adopt a multi-model collaborative automated annotation strategy, selecting five mainstream vision-language large models as annotators: GPT-5 Mini, Qwen2.5-VL-72B, Qwen3-VL-32B, Llama 3.2 90B Vision, and Gemini 2.0 Flash. Each model independently generates one caption, and their differing inference preferences and expression styles naturally produce caption diversity, providing rich language supervision signals for

of 45,000 annotated sentences. More details about UCCD are provided in the supplementary material.

5 Experiments

5.1 Evaluation Metrics and Datasets

Change Captioning: BLEU-1/2/3/4 [54] measure n-gram overlap; METEOR [55] considers synonyms and stemming matches; ROUGE-L [56] evaluates based on longest common subsequence; CIDEr-D [57] measures consistency with multiple reference texts and serves as the core metric. **Change Detection:** IoU [58] and F1-score [59] measure pixel-level overlap between predicted masks and ground truth masks. **Datasets:** **WHU-CDC** and **UCCD**.

5.2 Implementation Details

The proposed method trained on two NVIDIA A100 GPUs. We employ the AdamW optimizer with a global initial learning rate of $1e-4$, while the vision encoder and projection layers use a learning rate of $1e-5$, and weight decay coefficient is set to $5e-4$. Training proceeds for 200 epochs with a total batch size of 32. We apply LoRA with rank $r=16$ and $r=64$ to the CLIP vision encoder and Qwen2-1.5B language decoder, respectively. For WHU-CDC and UCCD, the number of prototype clusters K is set to 5 and 8, respectively, determined by the semantic diversity of change types in each dataset.

5.3 Comparison with State-of-the-Art Methods

Table 2 presents performance comparisons on WHU-CDC and UCCD. PTNet achieves state-of-the-art results on both benchmarks while maintaining a compact model size of 165.71M parameters.

WHU-CDC. PTNet achieves the best results on all seven metrics. Compared to the strongest baseline KCFI, B1 through B4 improve by 0.60, 0.62, 0.54, and 0.90, respectively, and METEOR improves by 0.74, reflecting more accurate semantic matching. Against Semantic-CC, B1 through B4 gains are 1.17, 1.57, 1.35, and 0.94. ROUGE-L at 79.64 and CIDEr-D at 150.02 remain competitive, validating caption structural quality and consistency with reference texts.

UCCD. PTNet again leads all metrics, with B1–B4 at 83.26, 75.35, 70.44, and 66.89, surpassing KCFI by 1.08, 0.73, 0.66, and 0.95, respectively, and METEOR reaching 44.15. CIDEr-D reaches 188.35, exceeding KCFI by 2.67, benefiting from UCCD’s five-caption-per-sample design. The generally elevated CIDEr-D scores on UCCD, for instance Prompt-CC achieves 184.82 compared to 134.50 on WHU-CDC, reflect richer reference annotations in this dataset.

Model Efficiency. With only 165.71M parameters, PTNet is significantly more compact than KCFI at 309.55M, Semantic-CC at 299.89M, and Chg2Cap at 285.50M, while outperforming all of them on every metric, demonstrating a strong accuracy–efficiency trade-off.

Table 2: Performance comparison. B1–B4: BLEU-1–4; MET: METEOR; R-L: ROUGE-L; CID: CIDEr-D. **Bold:** best result; underline: second best.

Method	WHU-CDC									UCCD									Train Params (M)
	B1	B2	B3	B4	MET	R-L	CID	F1	IoU	B1	B2	B3	B4	MET	R-L	CID	F1	IoU	
ChangeFormer [27]	-	-	-	-	-	-	-	86.11	77.88	-	-	-	-	-	-	-	68.03	50.46	41.03
SARAS-Net [60]	-	-	-	-	-	-	-	88.90	83.22	-	-	-	-	-	-	-	70.74	56.26	56.89
MCCFormers-S [61]	81.12	75.04	69.95	65.34	42.11	78.52	147.09	-	-	79.85	72.18	66.32	61.28	40.33	76.85	178.42	-	-	135.01
RSICFormer [62]	80.05	74.24	69.61	66.54	42.65	73.91	133.44	-	-	78.92	71.54	65.87	62.15	40.87	72.34	165.28	-	-	172.80
PSNet [63]	81.26	73.25	65.78	60.32	36.97	71.60	130.52	-	-	80.21	70.68	62.95	56.84	35.62	69.92	158.76	-	-	231.23
Prompt-CC [31]	81.12	73.96	67.22	61.45	36.99	71.88	134.50	-	-	81.13	72.49	65.11	58.22	38.28	71.00	184.82	-	-	196.28
Chg2Cap [30]	78.93	72.64	67.20	62.71	41.46	77.95	144.18	-	-	77.68	70.28	64.58	59.84	39.92	76.28	176.54	-	-	285.50
DiffusionRSCC [64]	75.32	70.15	66.40	63.76	40.18	73.80	127.96	-	-	74.26	67.82	63.75	60.94	38.65	72.14	155.42	-	-	58.42
Semantic-CC [34]	82.77	76.32	71.59	68.43	44.49	78.23	<u>150.23</u>	<u>88.46</u>	<u>84.95</u>	81.54	73.86	68.95	65.72	42.76	76.58	<u>186.47</u>	<u>71.94</u>	<u>56.45</u>	299.89
KCFI [35]	<u>83.34</u>	<u>77.27</u>	<u>72.40</u>	<u>68.47</u>	<u>44.95</u>	<u>79.59</u>	149.32	88.75	84.35	<u>82.18</u>	<u>74.62</u>	<u>69.78</u>	<u>65.94</u>	<u>43.28</u>	<u>78.12</u>	185.68	71.36	55.87	309.55
PTNet	83.94	77.89	72.94	69.37	45.69	79.64	150.02	89.77	86.27	83.26	75.35	70.44	66.89	44.15	78.47	188.35	72.77	57.65	165.71

Table 3: Ablation study on WHU-CDC and UCCD.

Configuration				WHU-CDC							UCCD						
Proto	TAMG	Det.	Guided \mathcal{L}_a	B-1	B-2	B-3	B-4	M	R-L	C	B-1	B-2	B-3	B-4	M	R-L	C
-	-	-	-	79.87	73.62	68.37	64.83	42.53	76.48	137.64	79.18	71.27	65.73	62.31	41.08	74.87	173.18
✓	-	-	-	81.43	75.31	70.28	66.68	43.76	77.73	142.57	80.79	72.83	67.58	64.08	42.29	76.28	179.06
✓	✓	-	-	82.68	76.58	71.63	67.93	44.68	78.61	146.13	81.97	74.03	68.87	65.41	43.17	77.31	183.47
✓	✓	✓	-	83.47	77.43	72.47	68.84	45.31	79.28	148.63	82.81	74.87	69.83	66.34	43.79	78.07	186.72
✓	✓	✓	✓	83.94	77.89	72.94	69.37	45.69	79.64	150.02	83.26	75.35	70.44	66.89	44.15	78.47	188.35

Figure 5 presents qualitative comparisons on both datasets. For each sample, we show the bi-temporal image pair, ground-truth mask (cd-GT), predicted mask (cd-infer), and captions from each method, with incorrect descriptions highlighted in red. Competing methods frequently produce hallucinated or spatially imprecise descriptions, such as misidentifying change locations or confusing change types, whereas PTNet generates more accurate and spatially faithful captions. This qualitative advantage stems from the explicit spatial priors injected by the detection branch via the mask encoder, and the cross-modal alignment enforced by the contrastive learning constraint. Notably, PTNet demonstrates robustness even in challenging cases such as partially occluded structures and densely built regions, where competing methods frequently produce location errors or hallucinated object descriptions.

Although change detection is an auxiliary task, our method achieves the high F1 and IoU. Against the specialized detector SARAS-Net, F1 improves by 2.03/0.87 on UCCD/WHU-CDC, showing that PG-CAI provides effective semantic priors for detection. Against joint-training methods KCFI and Semantic-CC, IoU improves by up to 1.32, attributed to TAMG supplying finer-grained spatial features for the detection branch while avoiding task-feature conflicts.

5.4 Ablation Studies

Component-wise Ablation We ablate each component, starting from a baseline using bi-temporal feature concatenation with shared representation.

Proto. Prototype-modulated cross-temporal attention yields the gain (B-4: +1.85/+1.77, CIDEr-D: +4.93/+5.88 on WHU-CDC/UCCD). Unlike simple

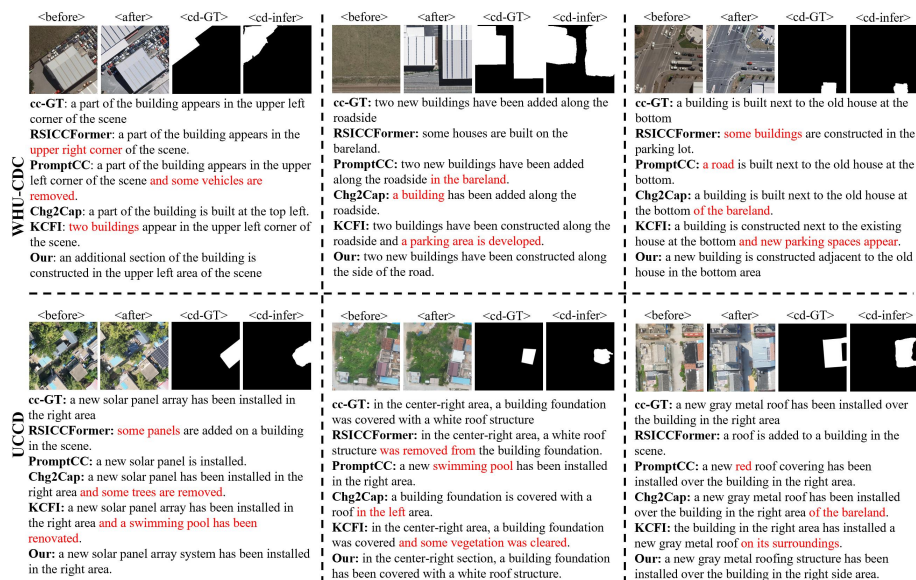


Fig. 5: Qualitative comparison on WHU-CDC and UCCD. Red text highlights erroneous or hallucinated descriptions.

Table 4: Left: Ablation on detection branch components (\checkmark / $-$: enabled/disabled). Right: Ablation on prototype modulation and initialization in PG-CAI.

Configuration				WHU-CDC				UCCD			
Det.	Dec.	TAMG	Det. G.	B-4	M	R-L	C	B-4	M	R-L	C
\checkmark	\checkmark	\checkmark	\checkmark	67.83	44.12	78.34	146.28	65.28	42.83	77.12	184.23
\checkmark	\checkmark	\checkmark	\checkmark	68.04	43.88	78.01	147.43	65.67	42.59	76.88	185.47
\checkmark	\checkmark	\checkmark	\checkmark	69.02	44.87	79.18	149.12	66.38	43.64	77.98	187.12
\checkmark	\checkmark	\checkmark	\checkmark	69.37	45.69	79.64	150.02	66.89	44.15	78.47	188.35

Configuration			WHU-CDC				UCCD			
Mod.	Init		B-4	M	R-L	C	B-4	M	R-L	C
w/o Modulation	\checkmark	\checkmark	67.85	44.21	78.65	146.83	65.32	43.18	77.45	185.12
Random Init	\checkmark	\checkmark	68.43	44.38	78.89	146.52	65.67	43.25	77.63	184.87
Proto. Init	\checkmark	\checkmark	69.37	45.69	79.64	150.02	66.89	44.15	78.47	188.35

feature subtraction, which treats all spatial positions equally, change-type prototypes provide structured semantic priors that steer cross-temporal attention toward semantically coherent regions, enabling more discriminative temporal correspondences.

TAMG. Task-adaptive gating further improves B-4 by 1.25/1.33. Without it, detection and captioning share identical representations, creating a granularity conflict between spatial precision and semantic abstraction. Head-level sigmoid gates disentangle these demands within a unified feature space, benefiting both tasks simultaneously.

Det. Guided. Injecting detection-derived spatial priors into the captioning branch yields consistent gains (B-4: +0.91/+0.93), as detection tokens explicitly supply *where* and *how extensively* change occurred— information that visual features alone cannot precisely convey.

\mathcal{L}_a . The contrastive alignment loss improves METEOR by +0.38/+0.36 and CIDEr-D by +1.39/+1.63. The pronounced METEOR gain reflects In-

Table 5: Performance comparison.

Method	WHU-CDC						UCCD						Params(M)
	B-4	MET	R-L	CID	F1	IoU	B-4	MET	R-L	CID	F1	IoU	
Chg2Cap	62.71	41.46	77.95	144.18	-	-	59.84	39.92	76.28	176.54	-	-	285.5
Prompt-CC	61.45	36.99	71.88	134.50	-	-	58.22	38.28	71.00	184.82	-	-	196.3
Semantic-CC	68.43	44.49	78.23	150.23	88.46	84.95	65.72	42.76	76.58	186.47	71.94	56.45	299.9
KCFI	68.47	44.95	79.59	149.32	88.75	84.35	65.94	43.28	78.12	185.68	71.36	55.87	309.5
PTNet (Ours)	69.37	45.69	79.64	150.02	89.77	86.27	66.89	44.15	78.47	188.35	72.77	57.65	165.7

foNCE’s nature: aligning visual representations to CLIP text embeddings cultivates synonym-aware semantics, which METEOR directly rewards.

Overall, PTNet surpasses the baseline by 4.54/4.58 in B-4 and 12.38/15.17 in CIDEr-D on WHU-CDC/UCCD. The larger CIDEr-D gain on UCCD stems from its five-caption-per-sample design, which amplifies the benefit of cross-modal alignment.

Analysis of Detection Branch Table 4 (left) ablates each component of the detection branch. Adding the detection decoder alone yields marginal captioning gains but slightly degrades METEOR, indicating feature competition between the two tasks without proper decoupling. TAMG resolves this conflict at the attention-head level, producing the largest improvement among the three components. Further incorporating detection-derived spatial priors via Det. Guided yields consistent gains across all metrics on both datasets, completing PTNet.

Analysis of Prototype Initialization in PG-CAI Table 4 (right) investigates prototype modulation and initialization strategy in PG-CAI. Removing prototype modulation causes consistent drops across all metrics (CIDEr-D: 150.02→146.83 on WHU-CDC), confirming that semantic modulation is essential for cross-temporal interaction. Random initialization reveals a telling dichotomy: n-gram metrics (B-4, ROUGE-L) slightly improve over the no-modulation baseline, yet semantic metrics (METEOR, CIDEr-D) degrade. This suggests random prototypes introduce spurious biases that improve lexical overlap while disrupting semantic coherence—indicating that prototype *quality* matters as much as their presence. Prototype-based initialization yields consistent gains across all metrics (CIDEr-D: +3.50/+3.48 on WHU-CDC/UCCD), confirming that semantically meaningful prototypes provide reliable modulation signals.

6 Conclusion

In this work, we advance the problem of urban change detection and captioning from both data and methodology perspectives. On the data side, we present UCCD, the first large-scale UAV-based benchmark designed for urban construction scenarios, covering diverse change types with high-resolution imagery and

multi-model collaborative annotations, providing the community with a valuable resource beyond existing satellite-based benchmarks. On the methodology side, we propose PTNet, which explicitly models change-type semantics via a learnable prototype bank, decouples the feature requirements of detection and captioning through task-adaptive gating, and bridges the two tasks by injecting detection-derived spatial priors into the caption generation process. Extensive experiments on WHU-CDC and UCCD demonstrate that PTNet achieves state-of-the-art performance on both tasks across all metrics. We hope this work inspires broader interest in fine-grained urban change understanding, moving beyond simple binary change masks toward spatially-aware and semantically-rich change descriptions.

references

- [1] Genc Hoxha, Saliha Chouaf, Farid Melgani, and Youcef Smara. Change captioning: A new paradigm for multitemporal remote sensing image analysis. *IEEE Transactions on Geoscience and Remote Sensing*, 60:1–14, 2022.
- [2] Duowang Zhu, Xiaohu Huang, Haiyan Huang, Hao Zhou, and Zhenfeng Shao. Change3d: Revisiting change detection and captioning from a video modeling perspective. In *Proceedings of the Computer Vision and Pattern Recognition Conference*, pages 24011–24022, 2025.
- [3] Xiliang Li, Bin Sun, Zhenhua Wu, Shutao Li, and Hu Guo. Cd4c: Change detection for remote sensing image change captioning. *IEEE Journal of Selected Topics in Applied Earth Observations and Remote Sensing*, 2025.
- [4] Chenyang Liu, Keyan Chen, Zipeng Qi, Zili Liu, Haotian Zhang, Zhengxia Zou, and Zhenwei Shi. Pixel-level change detection pseudo-label learning for remote sensing change captioning. In *IGARSS 2024-2024 IEEE International Geoscience and Remote Sensing Symposium*, pages 8405–8408. IEEE, 2024.
- [5] Wei Peng, Ping Jian, Zhuqing Mao, and Yingying Zhao. Change captioning for satellite images time series. *IEEE Geoscience and Remote Sensing Letters*, 21:1–5, 2024.
- [6] Ashish Vaswani, Noam Shazeer, Niki Parmar, Jakob Uszkoreit, Llion Jones, Aidan N. Gomez, Łukasz Kaiser, and Illia Polosukhin. Attention is all you need. In *Advances in Neural Information Processing Systems (NeurIPS)*, volume 30, pages 5998–6008, 2017.
- [7] Alexey Dosovitskiy, Lucas Beyer, Alexander Kolesnikov, Dirk Weissenborn, Xiaohua Zhai, Thomas Unterthiner, Mostafa Dehghani, Matthias Minderer, Georg Heigold, Sylvain Gelly, Jakob Uszkoreit, and Neil Houlsby. An image is worth 16x16 words: Transformers for image recognition at scale. In *International Conference on Learning Representations (ICLR)*, 2021.
- [8] Lingwu Meng, Jing Wang, Yan Huang, and Liang Xiao. Rsic-gmamba: A state space model with genetic operations for remote sensing image captioning. *IEEE Transactions on Geoscience and Remote Sensing*, 2025.
- [9] Dongwei Sun, Jing Yao, Wu Xue, Changsheng Zhou, Pedram Ghamisi, and Xiangyong Cao. Mask approximation net: A novel diffusion model approach

- for remote sensing change captioning. *IEEE transactions on geoscience and remote sensing*, 2025.
- [10] Bin Zhang, Shuting Zhao, Yuqi Liang, Jiaming Ye, Shuai Lu, and Jiawei Ma. RS-LLaVA: A large vision-language model for joint captioning and question answering in remote sensing imagery. *Remote Sensing*, 16(9):1477, 2024.
- [11] Javier Lamar León, Vitor Nogueira, Pedro Salgueiro, and Paulo Quaresma. Describing land cover changes via multi-temporal remote sensing image captioning using llm, vit, and lora. *Remote Sensing*, 18(1):166, 2026.
- [12] Simon Vandenhende, Stamatios Georgoulis, Wouter Van Gansbeke, Marc Proesmans, Dengxin Dai, and Luc Van Gool. Multi-task learning for dense prediction tasks: A survey. *IEEE Transactions on Pattern Analysis and Machine Intelligence*, 44(7):3614–3633, 2021.
- [13] Jingye Shi, Mengge Zhang, Yuwu Hou, Ruicong Zhi, and Jiqiang Liu. A multitask network and two large-scale datasets for change detection and captioning in remote sensing images. *IEEE Transactions on Geoscience and Remote Sensing*, 62:1–17, 2024.
- [14] Xiliang Li, Bin Sun, and Shutao Li. Detection assisted change captioning for remote sensing image. In *IGARSS 2024-2024 IEEE International Geoscience and Remote Sensing Symposium*, pages 10454–10458. IEEE, 2024.
- [15] Chenyang Liu, Keyan Chen, Haotian Zhang, Zipeng Qi, Zhengxia Zou, and Zhenwei Shi. Change-agent: Toward interactive comprehensive remote sensing change interpretation and analysis. *IEEE Transactions on Geoscience and Remote Sensing*, 62:1–16, 2024.
- [16] Dongwei Sun, Yuduo Wang, Jing Yao, Weikang Yu, Xiangyong Cao, and Pedram Ghamisi. Scnet: Lightweight spatial-channel attention network for remote sensing change captioning. *IEEE Transactions on Geoscience and Remote Sensing*, 2026.
- [17] Chenyang Liu, Jiafan Zhang, Keyan Chen, Man Wang, Zhengxia Zou, and Zhenwei Shi. Remote sensing spatiotemporal vision–language models: A comprehensive survey. *IEEE Geoscience and Remote Sensing Magazine*, 2025.
- [18] Alec Radford, Jong Wook Kim, Chris Hallacy, Aditya Ramesh, Gabriel Goh, Sandhini Agarwal, Girish Sastry, Amanda Askell, Pamela Mishkin, Jack Clark, Gretchen Krueger, and Ilya Sutskever. Learning transferable visual models from natural language supervision. In *Proceedings of the International Conference on Machine Learning (ICML)*, pages 8748–8763, 2021.
- [19] Aaron van den Oord, Yazhe Li, and Oriol Vinyals. Representation learning with contrastive predictive coding. *arXiv preprint arXiv:1807.03748*, 2018.
- [20] Sheng Fang, Kaiyu Li, Jinyuan Shao, and Zhe Li. SNUNet-CD: A densely connected siamese network for change detection of VHR images. *IEEE Geoscience and Remote Sensing Letters*, 19:1–5, 2022.
- [21] Kaiming He, Xiangyu Zhang, Shaoqing Ren, and Jian Sun. Deep residual learning for image recognition. In *Proceedings of the IEEE Conference on Computer Vision and Pattern Recognition (CVPR)*, pages 770–778, 2016.

- [22] Rodrigo Caye Daudt, Bertrand Le Saux, and Alexandre Boulch. Fully convolutional siamese networks for change detection. In *Proceedings of the IEEE International Conference on Image Processing (ICIP)*, pages 4063–4067, 2018.
- [23] Hao Chen and Zhenwei Shi. A spatial-temporal attention-based method and a new dataset for remote sensing image change detection. *Remote Sensing*, 12(10):1662, 2020.
- [24] Ze Liu, Yutong Lin, Yue Cao, Han Hu, Yixuan Wei, Zheng Zhang, Stephen Lin, and Baining Guo. Swin transformer: Hierarchical vision transformer using shifted windows. In *Proceedings of the IEEE/CVF International Conference on Computer Vision (ICCV)*, pages 10012–10022, 2021.
- [25] Mustansar Noman, Mustansar Fiaz, Hisham Cholakkal, Rao Muhammad Anwer, Salman Khan, and Fahad Shahbaz Khan. Remote sensing change detection with transformers trained from scratch. *IEEE Transactions on Geoscience and Remote Sensing*, 62:1–15, 2024.
- [26] Hao Chen, Zipeng Qi, and Zhenwei Shi. Remote sensing image change detection with transformers. *IEEE Transactions on Geoscience and Remote Sensing*, 60:1–14, 2021.
- [27] Wele Gedara Chaminda Bandara and Vishal M. Patel. A transformer-based siamese network for change detection. In *Proceedings of the IEEE International Geoscience and Remote Sensing Symposium (IGARSS)*, pages 207–210, 2022.
- [28] Yunpeng Li, Xiangrong Zhang, Xina Cheng, Puhua Chen, and Licheng Jiao. Intertemporal interaction and symmetric difference learning for remote sensing image change captioning. *IEEE Transactions on Geoscience and Remote Sensing*, 62:1–13, 2024.
- [29] Chenyang Liu, Rui Zhao, Hao Chen, Zhengxia Zou, and Zhenwei Shi. Remote sensing image change captioning with dual-branch transformers: A new method and a large scale dataset. *IEEE Transactions on Geoscience and Remote Sensing*, 60:1–20, 2022.
- [30] Shizhen Chang and Pedram Ghamisi. Changes to captions: An attentive network for remote sensing change captioning. *IEEE Transactions on Image Processing*, 32:6047–6060, 2023.
- [31] Chenyang Liu, Rui Zhao, Jianqi Chen, Zipeng Qi, Zhengxia Zou, and Zhenwei Shi. A decoupling paradigm with prompt learning for remote sensing image change captioning. *IEEE Transactions on Geoscience and Remote Sensing*, 61:1–18, 2023.
- [32] Chenyang Liu, Keyan Chen, Bowen Chen, Haotian Zhang, Zhengxia Zou, and Zhenwei Shi. RSCaMa: Remote sensing image change captioning with state space model. *IEEE Geoscience and Remote Sensing Letters*, 21:1–5, 2024.
- [33] Yunpeng Yang, Tingting Liu, Yonggang Pu, Lianming Liu, Qing Zhao, and Qian Wan. Remote sensing image change captioning using multi-attentive network with diffusion model. *Remote Sensing*, 16(21):4083, 2024.
- [34] Haoran Liu, Yibo Zhao, Yuan Jin, Keyan Li, Jiaqi Chen, Zhengxia Zou, and Zhenwei Shi. Semantic-CC: Boosting remote sensing image change cap-

- tioning via foundational knowledge and semantic guidance. *arXiv preprint arXiv:2407.14032*, 2024.
- [35] Cong Yang, Zuchao Li, Hongzan Jiao, Zhi Gao, and Lefei Zhang. Enhancing perception of key changes in remote sensing image change captioning. *IEEE Transactions on Image Processing*, 2025.
- [36] Haotian Liu, Chunyuan Li, Qingyang Wu, and Yong Jae Lee. Visual instruction tuning. In *Advances in Neural Information Processing Systems (NeurIPS)*, 2023.
- [37] Junnan Li, Dongxu Li, Silvio Savarese, and Steven Hoi. BLIP-2: Bootstrapping language-image pre-training with frozen image encoders and large language models. In *Proceedings of the International Conference on Machine Learning (ICML)*, pages 19730–19742, 2023.
- [38] Di Wang, Qiming Zhang, Yanxing Xu, Jing Zhang, Bo Du, Dacheng Tao, and Liangpei Zhang. Advancing plain vision transformer towards remote sensing foundation model. *IEEE Transactions on Geoscience and Remote Sensing*, 61:1–15, 2023.
- [39] Sylvain Lobry, Diego Marcos, Jesse Murray, and Devis Tuia. RSVQA: Visual question answering for remote sensing data. *IEEE Transactions on Geoscience and Remote Sensing*, 58(12):8555–8566, 2020.
- [40] Kartik Kuckreja, Muhammad Sohail Danish, Muzammal Naseer, Abhijit Khan, Salman Khan, and Fahad Shahbaz Khan. GeoChat: Grounded large vision-language model for remote sensing. In *Proceedings of the IEEE/CVF Conference on Computer Vision and Pattern Recognition (CVPR)*, pages 27831–27840, 2024.
- [41] Yunpeng Wang, Wenbo Li, Jian Gong, Michael Kopp, and Devis Tuia. EarthVQA: Towards queryable earth via relational reasoning-based remote sensing visual question answering. *arXiv preprint arXiv:2312.12222*, 2023.
- [42] Pei Deng, Wenqian Zhou, and Hanlin Wu. ChangeChat: An interactive model for remote sensing change analysis via multimodal instruction tuning. *arXiv preprint arXiv:2409.08582*, 2025.
- [43] Mustansar Noman, Noor Ahsan, Muzammal Naseer, Hisham Cholakkal, Rao Muhammad Anwer, Salman Khan, and Fahad Shahbaz Khan. CDChat: A large multimodal model for remote sensing change description. *arXiv preprint arXiv:2409.16261*, 2024.
- [44] Yujie Li et al. BTCChat: Advancing remote sensing bi-temporal change captioning with multimodal large language model. *arXiv preprint arXiv:2509.05895*, 2025.
- [45] Yuchao Wang, Wele Gedara Chaminda Yu, Michael Kopp, and Devis Tuia. ChangeMinds: Multi-task framework for detecting and describing changes in remote sensing. *arXiv preprint arXiv:2410.10047*, 2024.
- [46] Edward J. Hu, Yelong Shen, Phillip Wallis, Zeyuan Allen-Zhu, Yuanzhi Li, Shean Wang, Lu Wang, and Weizhu Chen. LoRA: Low-rank adaptation of large language models. In *International Conference on Learning Representations (ICLR)*, 2022.
- [47] Tsung-Yi Lin, Piotr Dollár, Ross Girshick, Kaiming He, Bharath Hariharan, and Serge Belongie. Feature pyramid networks for object detection.

- In *Proceedings of the IEEE Conference on Computer Vision and Pattern Recognition (CVPR)*, pages 2117–2125, 2017.
- [48] Zhang Chen, Shuai Wan, Siyu Ren, Fuzheng Yang, Mengting Yu, and Junhui Hou. Rbfim: Perceptual quality assessment for compressed point clouds using radial basis function interpolation. *IEEE Transactions on Multimedia*, 27:8579–8591, 2025.
- [49] Shikun Liu, Edward Johns, and Andrew J. Davison. End-to-end multi-task learning with attention. In *Proceedings of the IEEE Conference on Computer Vision and Pattern Recognition (CVPR)*, pages 1871–1880, 2019.
- [50] Philipp Lindenberger, Paul-Edouard Sarlin, and Marc Pollefeys. Lightglue: Local feature matching at light speed. In *Proceedings of the IEEE/CVF international conference on computer vision*, pages 17627–17638, 2023.
- [51] Kunping Yang, Jianchong Wei, Chengbin Chen, Zhensheng Wang, Junhui Lan, Xuanping Li, Duwei Hua, Dingli Xue, and Yi Wu. Restricted supervised cascade information network for remote sensing change captioning with serial sentences. *International Journal of Applied Earth Observation and Geoinformation*, 142:104686, 2025.
- [52] Jingye Shi, Mengge Zhang, Yewu Hou, Ruicong Zhi, and Jiqiang Liu. A multitask network and two large-scale datasets for change detection and captioning in remote sensing images. *IEEE Transactions on Geoscience and Remote Sensing*, 62:1–17, 2024.
- [53] Ali Can Karaca, Enes Ozelbas, Saadettin Berber, Orkhan Karimli, Turabi Yildirim, and Mehmet Fatih Amasyali. Robust change captioning in remote sensing: SECOND-CC dataset and MModalCC framework. *IEEE Journal of Selected Topics in Applied Earth Observations and Remote Sensing*, 18:21494–21513, 2025.
- [54] Kishore Papineni, Salim Roukos, Todd Ward, and Wei-Jing Zhu. Bleu: a method for automatic evaluation of machine translation. In *Proceedings of the 40th Annual Meeting of the Association for Computational Linguistics*, pages 311–318, Philadelphia, Pennsylvania, USA, July 2002. Association for Computational Linguistics.
- [55] Satyanjeev Banerjee and Alon Lavie. METEOR: An automatic metric for MT evaluation with improved correlation with human judgments. In *Proceedings of the ACL Workshop on Intrinsic and Extrinsic Evaluation Measures for Machine Translation and/or Summarization*, pages 65–72, Ann Arbor, Michigan, June 2005. Association for Computational Linguistics.
- [56] Chin-Yew Lin. ROUGE: A package for automatic evaluation of summaries. In *Text Summarization Branches Out*, pages 74–81, Barcelona, Spain, July 2004. Association for Computational Linguistics.
- [57] Ramakrishna Vedantam, C. Lawrence Zitnick, and Devi Parikh. CIDEr: Consensus-based image description evaluation. In *Proceedings of the IEEE Conference on Computer Vision and Pattern Recognition (CVPR)*, pages 4566–4575, 2015.
- [58] Dingfu Zhou, Jin Fang, Xibin Song, Chenye Guan, Junbo Yin, Yuchao Dai, and Ruigang Yang. Iou loss for 2d/3d object detection. In *2019 international conference on 3D vision (3DV)*, pages 85–94. IEEE, 2019.

- [59] Nafiseh Ghasemian Sorboni, Jinfei Wang, and Mohammad Reza Najafi. Fusion of google street view, lidar, and orthophoto classifications using ranking classes based on f1 score for building land-use type detection. *Remote Sensing*, 16(11):2011, 2024.
- [60] Chao-Peng Chen, Jun-Wei Hsieh, Ping-Yang Chen, Yi-Kuan Hsieh, and Bor-Shiun Wang. Saras-net: Scale and relation aware siamese network for change detection. In *Proceedings of the AAAI Conference on Artificial Intelligence*, volume 37, pages 14187–14195, 2023.
- [61] Yue Qiu, Shintaro Yamamoto, Kazutoshi Nakashima, Ryota Suzuki, Kenji Iwata, Hirokatsu Kataoka, and Yutaka Satoh. Describing and localizing multiple changes with transformers. In *Proceedings of the IEEE/CVF International Conference on Computer Vision (ICCV)*, pages 1951–1960, 2021.
- [62] Chenyang Liu, Rui Zhao, Hao Chen, Zhengxia Zou, and Zhenwei Shi. Remote sensing image change captioning with dual-branch transformers: A new method and a large scale dataset. *IEEE Transactions on Geoscience and Remote Sensing*, 60:1–20, 2022.
- [63] Chenyang Liu, Jiajun Yang, Zipeng Qi, Zhengxia Zou, and Zhenwei Shi. Progressive scale-aware network for remote sensing image change captioning. In *IGARSS 2023-2023 IEEE International Geoscience and Remote Sensing Symposium*, pages 6668–6671. IEEE, 2023.
- [64] Xiaofei Yu, Yitong Li, Jie Ma, Chang Li, and Hanlin Wu. Diffusion-RSCC: Diffusion probabilistic model for change captioning in remote sensing images. *IEEE Transactions on Geoscience and Remote Sensing*, 2025.